Advances in Nanochemistry
ISSN: 2676-5462

Research

Turn-on fluorescent detection of polycyclic aromatic hydrocarbons (PAHs) based on glutathione-capped CdTe/ZnS core/shell quantum dot (QDs)–graphene oxide (GO) nanocomposite: experimental and computational studies

Marzieh Sadeghi *[1], Saba Hadidi[2], Tahereh Shokri[1]

[1] Department Chemistry, Razi University, Kermanshah, Iran
[2] Department of Inorganic Chemistry, Faculty of Chemistry, Razi University, Kermanshah, Iran

Received 21st July 2021,
Accepted 20th October 2021,
DOI: 10.22126/anc.2021.6722.1030

Abstract

Polycyclic aromatic hydrocarbons (PAHs) are ubiquitous pollutants in our environment and their importance appears from their toxicity and carcinogenicity to humans. Water can become contaminated with PAHs from different sources such as runoff in urban areas, wastewater from specific industries, and petroleum spills. Herein, an efficient turn-on fluorescence sensor, based on covalently-linked glutathione (GSH)-capped CdTe/ZnS core/shell quantum dot (QDs)–graphene oxide (GO) nanocomposite was developed for PAHs sensing. The fluorescence emission of the QDs–GO nanocomposite was increased relative to the unconjugated QDs. Various techniques including TEM, SEM, XRD, FT-IR, UV/Vis, and fluorescence spectrophotometry were employed to characterize the QDs and the QDs–GO nanocomposite. Naphthalene, as a model of PAHS, was selected for further studies as the fluorescence enhancement. A limit of detection (LOD) of 7.71 × 10^{-8} mol L^{-1} was obtained for naphthalene under optimum conditions.

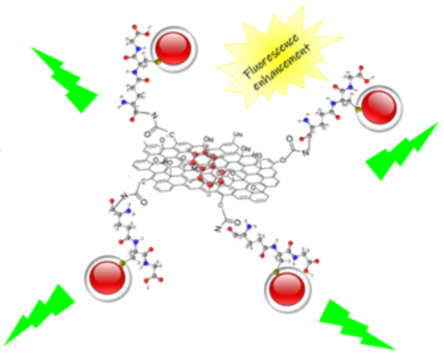

Keywords: *Glutathione (GSH)-capped CdTe/ZnS core/shell quantum dot, Graphene oxide, Turn-on fluorescence probe, Polycyclic aromatic hydrocarbons.*

Introduction

Quantum dots (QDs) have attracted the attention of many researchers in recent years. In comparison to organic dyes and fluorescent proteins, QDs have unique functional and structural properties, such as high fluorescence quantum yields, large absorption cross-sections, narrow and Gaussian emission spectra, size and composition tunable emission, and high photobleaching threshold. Earlier studies related to the interactions between QDs and some compounds, for instance, the interactions with vitamin B_{12} and hemoglobin had revealed that the reactions would change the photophysical properties of QDs.[1]

Polycyclic aromatic hydrocarbons (PAHs) are organic compounds that are mostly white, colorless, or pale yellow solids. They are a ubiquitous group of several hundred chemically related compounds, environmentally persistent with various toxicity and structures. They have toxic effects on organisms through various actions. Generally, PAHs enter the environment through various routes and are usually found as a mixture containing two or more of these compounds. The term ‘‘PAH” refers to compounds consisting of only hydrogen and carbon atoms. Chemically the PAHs are comprised of two or more benzene rings bonded in the linear, cluster, or angular arrangements. The major source of PAHs is the incomplete combustion of organic materials such as oil, coal, and wood.[2,3] Hence, the presence of PAHs in the environment is of health concern[4] and requires extensive monitoring. High-performance gas chromatography (GC) and liquid chromatography (HPLC) are typically working for the environmental monitoring of PAHs. While these methods have proven successful, they often require analyte extraction and cleanup before analysis.[5] The development of rapid, simple, sensitive, and selective methods for screening environmental samples for PAHs is, therefore, an attractive alternative. Newly, carbon-based materials such as graphene and graphene oxide (GO), which exhibit a single sp^2 layered hybridized carbon atom bonded in a covalent honeycomb-like crystal lattice, has emerged as a suitable adsorbent material for

---

**Corresponding authors:* Marzieh Sadeghi, Email: negarsade@gmail.com and m.sadeghi@razi.ac.ir

Cite this article: Sadeghi, M., Hadidi, S., & Shokri, T. (2021). Turn-on fluorescent detection of polycyclic aromatic hydrocarbons (PAHs) based on glutathione-capped CdTe/ZnS core/shell quantum dot (QDs)–graphene oxide (GO) nanocomposite: experimental and computational studies. *Advances in Nanochemistry*, 3(2), 63-70. DOI: 10.22126/anc.2021.6722.1030

Publisher: Razi University

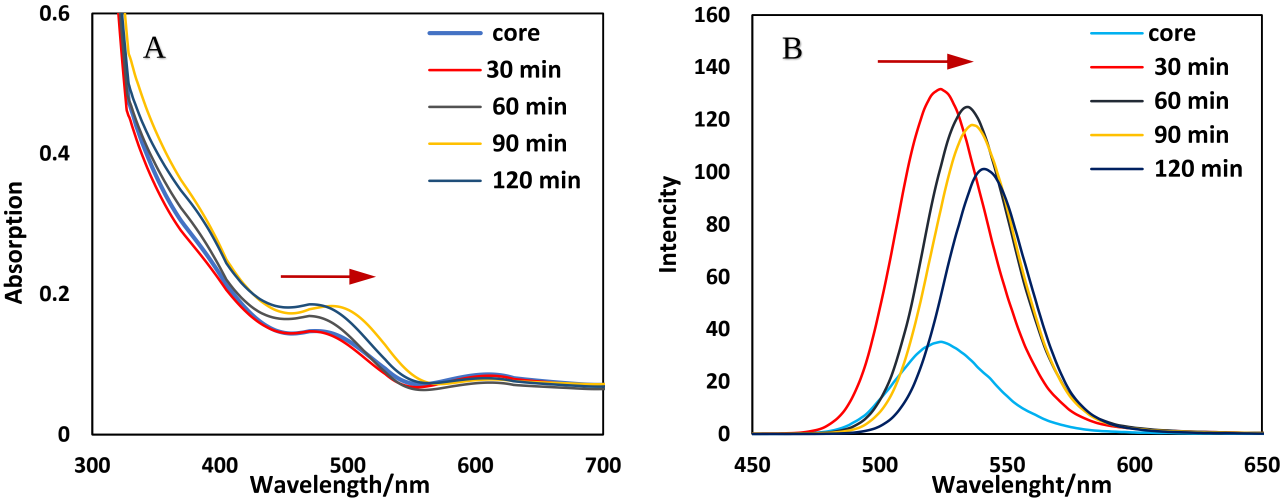

***Figure 1**. (A) UV/Vis absorption and (B) fluorescence emission spectra of core CdTe QDs and GSH-CdTe/ZnS core/shell QDs with a different growing times of shell layers for 30, 60, 90 and, 120 min, respectively. The concentration was, 8.80 × 10^{-6} M, λ_{ex}=380 nm.*

the preconcentration of several environmental organic pollutants containing fused benzene rings from both air and water matrices.[6,7] The superior adsorptive influence of graphene-based materials is due to their high surface area, and large delocalized π electrons.[8]

Bonding of QDs to graphene-based materials to form nanocomposite probes for the detection of analytes such as chloramphenicol,[9] lead ions,[10] and glucose[11] have been reported. In this work, we have successfully synthesized CdTe/ZnS QDs core/shell nanoparticles. The selection of the alloyed QDs core and the passivation with a Zn-based shell ensure the Cd ion is powerfully protected against leakage, hence guaranteeing the QDs do not pose any form of environmental impact or toxicity in use. To form novel QDs–GO nanocomposite, the synthesized QDs were covalently bonded to GO, which we investigated for use as a fluorescent probe to detect commonly found PAHs in water. The simplicity of the newly developed QDs–GO nanocomposite sensor takes advantage of the adsorptive power and delocalized π interactions of graphene. These features enhance adsorption of PAHs compounds with consequent enhancement of the QDs fluorescence.

Experimental

Reagents and chemicals

All chemical reagents were of analytical grade and used without further purification. Sodium borohydride ($NaBH_4$), sodium hydrogen phosphate (Na_2HPO_4), potassium dihydrogen phosphate (KH_2PO_4), cadmium chloride monohydrate ($CdCl_2.H_2O$), rhodamine 6G, glutathione (GSH), sodium nitrate ($NaNO_3$), 1-ethyl-3-(3-dimethylaminopropyl) carbodiimide hydrochloride (EDC), N-hydroxysuccinimide (NHS) were bought from Sigma-Aldrich Chemical Company. Tellurium powder, thioglycolic acid (TGA), sodium hydroxide (NaOH), ethanol (C_2H_5OH), sulfuric acid 98%, potassium manganate (VII) ($KMnO_4$), naphthalene, and hydrogen peroxide (H_2O_2) were procured from Merck (Darmstadt, Germany). All solution was prepared using deionized water.

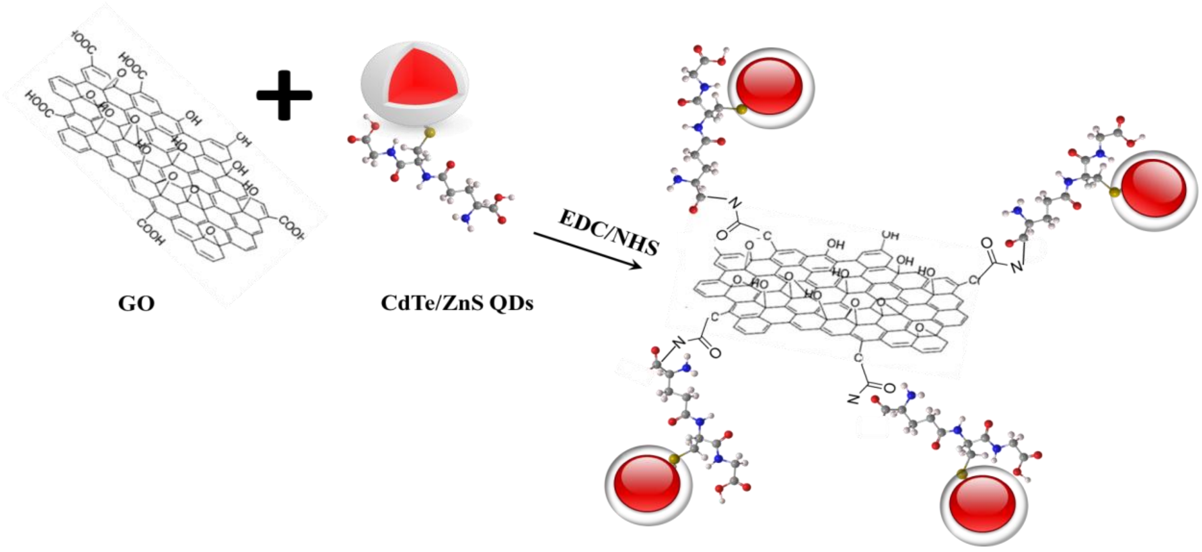

***Scheme 1.** Schematic representation of the synthesis route for the QDs–GO nanocomposite.*

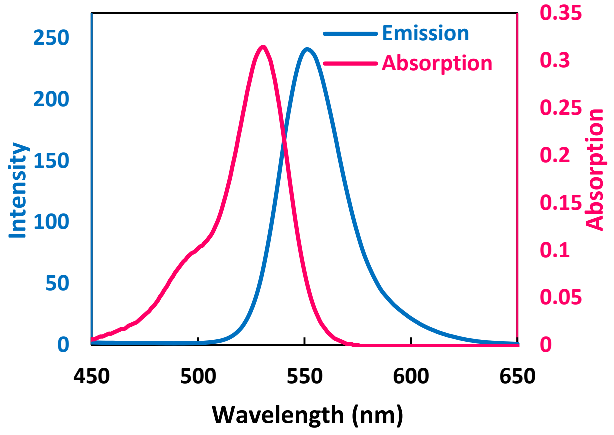

***Figure 2**. Absorption and emission spectra of the rhodamine in ethanol, λ_{ex} =380 nm.*

Apparatus and Measurement

All fluorescence measurements were performed by a JASCO FP-6200 spectrofluorometer equipped with a quartz cell (1 cm×1 cm). Excitation and emission slits were set at 5 and 10 nm, respectively. UV/Vis spectra were carried out by a NORDANTEC T180 diode array spectrophotometer at the range of 220-800 nm. The Fourier-transform infrared (FT-IR) spectra of core and core/shell QDs were recorded over the range from 500 to 4000 cm^{-1} on a Shimadzu infrared spectrophotometer. Powder X-ray diffraction (XRD) patterns were recorded by Panalytical X'PertPro (40 kV, 30 mA) XRD equipped Cu Kα radiation source (λ=1.542 Å) and a nickel filter in the 2θ range of 10°-90°. Peak location was compared with standard files to obtain the similarity of the crystalline phase. Samples for recording FT-IR, XRD, and high-resolution transmission electron microscopy (HRTEM) were dried by Alpha 2-4 LD-Christ Freeze dryer at −85 ℃. All pH measurement was reported by JENWAY (3345) pH meter at room temperature. The morphology of GO was studied using a TSCAN Mira 3-XMU cold field-emission scanning electron microscope (FE-SEM). The morphology of the core/shell was examined by an FEI, TEC9G20 HRTEM.

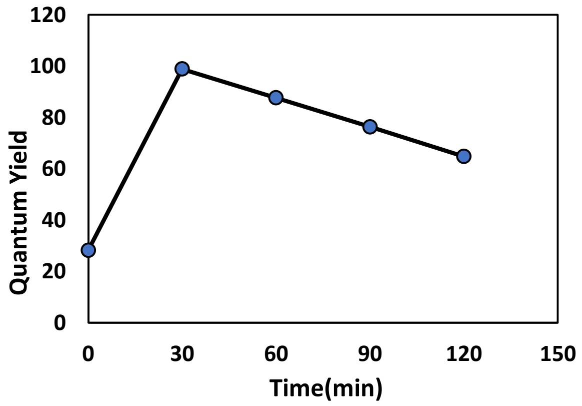

***Figure 3.** Fluorescence QY of the CdTe QDs and GHS-CdTe/ZnS at different synthesis times.*

Computational details

Energy Decomposition Analysis (EDA) was done using ORCA, version 4.2,[12] and NBO codes with the Grimme dispersion corrected B3LYP functional[13,14] using 6-311G(d,p) basis set for all atoms. Time-dependent density-functional based tight-binding (TD-DFTB) was used to calculate the UV/Vis absorption and fluorescence emission spectra by means of the DFTB+ program[14] and Quasinano 2015 parameters.[15,16]

Syntheses of GO

GO nanosheets were prepared based on the modified Hummers method.[17,18] Briefly, in a 250 mL round bottom flask, 35 mL of H_2SO_4 was added, then 0.5 g of graphite powder and 0.5 g of $NaNO_3$ were added and the solution was vigorously stirred to allow for thorough dispersion of the graphite powder for 12 h. Afterward, 4 g of $KMnO_4$ was slowly added, and the solution was kept on ice for a few hours. Thereafter, the ice bath was removed and their action mixture was stirred under ambient temperature overnight, which resulted in the formation of a pasty light brown colored mixture. The following day, 120 mL of Millipore water was slowly added under stirring at room temperature. Then, 3 mL of 30% H_2O_2 was added to the reaction mixture to remove manganese oxides byproducts. Then, to form the GO nanosheets, the mixture solution (graphite oxide) was exfoliated via ultra-sonication for 3 h. Finally, the solution was washed with water several times, centrifuged, and dried at 65 °C.

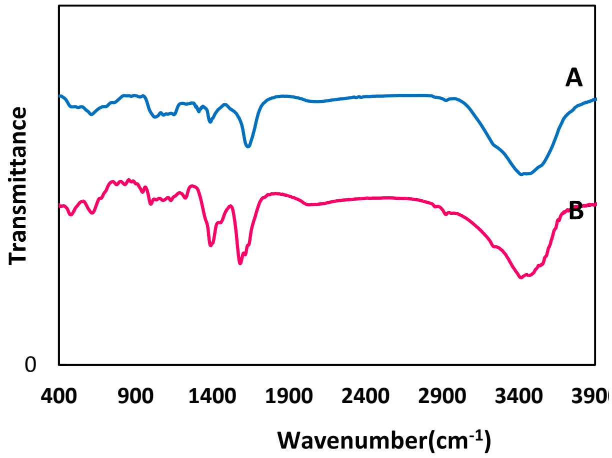

***Figure 4.** FT-IR spectra of (A) CdTe and (B) GHS-CdTe/ZnS.*

Synthesis of GSH-capped CdTe/ZnS core/shell QDs

Synthesis of TGA-CdTe QDs was performed according to the previous report. Firstly, NaHTe was prepared by adding 10 mg $NaBH_4$ to a flask containing 13 mg tellurium powder and 4 mL double distilled water under a nitrogen atmosphere. To reduce all tellurium, the solution was stirred for several hours until the violet color of the solution was removed. In the next step, 80 mg of $CdCl_2$ and 44 µL of TGA were dissolved in 100 mL double distilled water, followed by adjusting the pH to 11.0 by adding enough amount of NaOH solution (0.5 M).

The NaTeH solution was quickly injected into the degassed solution of Cd^{2+} and TGA under vigorous stirring. The mixture of Cd^{2+}, NaHTe, and TGA was heated at 100 °C for 30 min in a reflux system under a nitrogen atmosphere. The obtained solution was washed with ethanol and centrifuged for 15 min at 4000 rpm to remove excess Cd^{2+} and TGA. Then, the precipitate was redissolved in proper Zn^{2+} and GSH solution, and the process of preparation was repeated to remove excess Cd^{2+} on surfaces of CdTe QDs.

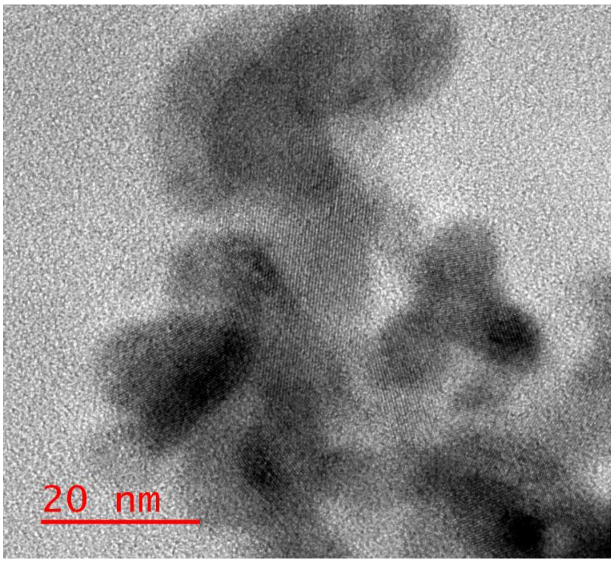

Figure 5. *HRTEM image of GSH-CdTe/ZnS QDs.*

For synthesis of CdTe/ZnS core/shell QDs, as-prepared CdTe QDs were added to the 50 mL solution (pH 8) containing 1 mmol L^{-1} $ZnCl_2$ (7 mg) and 4 mmol L^{-1} GSH (61 mg). The solution was heated to 100 °C under open-air conditions and refluxed from 10 min to 2 h for controlling the sizes of core/shell QDs. Finally, the obtained CdTe/ZnS QDs were dried by freeze-drying technology at the temperature −85 °C for characterization. The concentration of the GSH-CdTe/ZnS solution was evaluated by the experimental formula as equations 1-2 and 2-2 as 8.80×10^{-6} M according to a reported method.[19]

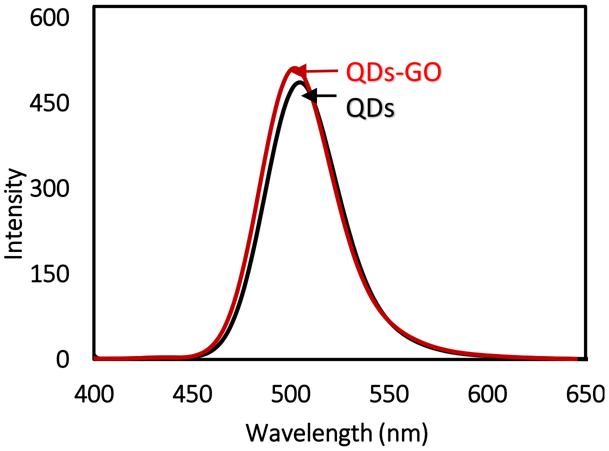

Figure 6. *The emission spectra of the unconjugated QDs and conjugation QDs-GO at λ_{ex} =380 nm.*

Synthesis of QDs–GO solution

To prepare of the QDs–GO solution, firstly, 100 μL GO solution was added to 1700 μL PBS (pH 7.5, 25 mM). Then 10 μL of 3.20×10^{-3} $mol\ L^{-1}$ EDC was added to the GO solution to activate the carboxylic groups for 5 min. 200 μL of the GSH-capped CdTe/ZnS QDs (8.80×10^{-6} M) solution was then added into the EDC-activated GO solution, immediately followed by the addition of 10 μL of 4.30×10^{-3} $mol\ L^{-1}$ NHS solution to stabilize the amide linkage formed between the QDs and GO.[20] The synthesis route of QDs–GO nanocomposite is displayed in Scheme 1.

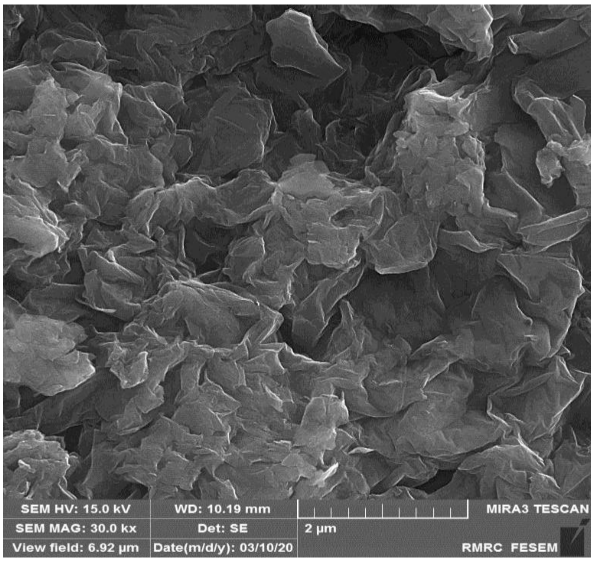

Figure 7. *FESEM image of GO.*

General procedure

The stock solution of rhodamine was prepared by dissolving an appropriate amount of rhodamine in ethanol, and this solution was used as a reference to taken emission and absorption spectra for calculation of fluorescence quantum yields (QY) of CdTe and CdTe/ZnS QDs. For preparation of EDC (M_w=155.24 g mol^{-1}) and NHS (M_w=115.09 g mol^{-1}) solution, 5 mg of EDC and 5 mg of NHS were dissolved in 10 mL deionized water. The stock solution of naphthalene (M_w=178.23 g mol^{-1}) was prepared in an H_2O/EtOH (2:1) mixture (2.50×10^{-4} $mol\ L^{-1}$). GO solution was prepared by dissolving 1 mg GO powder in 10 mL deionized water and sonication for 30 min. For fluorescence detection of naphthalene, varying concentrations of naphthalene solution were added to QDs–GO solution, and an equilibration time of 5 min was allowed before taking each emission measurement.

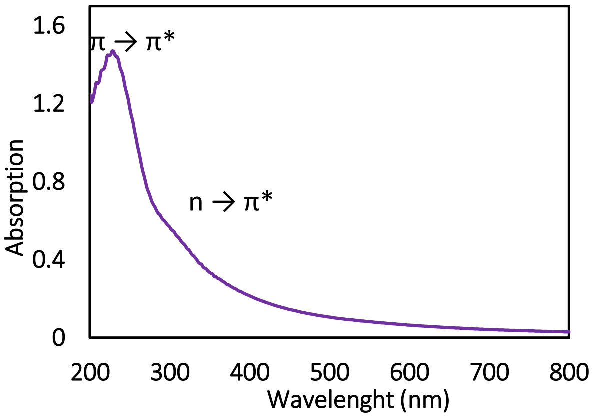

Figure 8. *UV/Vis spectra of the aqueous solution of GO (1.00× 10^2 mg/L) at room temperature.*

Results and discussion

Characterization of GSH-CdTe/ZnS QDs

The absorption and emission spectra for CdTe and GHS-CdTe/ZnS were shown in Figure 1. With increasing the reflux time, the absorption and emission spectra slowly red shift. The maximum emission was shown in reflux time 30 min. With increasing reflux time to 60, 90, and 120 min, the emission value was decreased, respectively. According to equation 1 and equation 2, the size and concentration of GSH-CdTe/ZnS QDs in reflux time 30 min are 12.70 nm and 8.80×10^{-6} M.

$$A = \varepsilon bc \qquad \varepsilon = 10043\ (D)^{2.12} \tag{1}$$

$$D = (9.8127 \times 10^{27})\lambda^3 - (1.7147 \times 10^{-3})\lambda^2 + (1.0064)\lambda - (194.84) \tag{2}$$

A compressive ZnS layer wrapped the CdTe core, which formed a lattice-mismatched Type-I core/shell heterostructure QDs could obtain high-quality luminescent properties.[21] As shown in Figure 1 A, the absorption peak for GHS-CdTe/ZnS QDs was at 505 nm, and the excitonic absorption was strong. Under the condition of excitation wavelengths of 380 nm, the fluorescence spectrum of QDs recognized that the full width half maximum was narrow and showed good balance, and the fluorescence band was centered at 523 nm.

Luminescent materials convert excitation energy into photons, and this conversion is usually not 100% efficient due to various losses occurring through alternative deactivation paths. Therefore, two additional parameters have to be defined, the quantum yield and the quantum (energy) efficiency. In the research, the fluorescence QY of our sample was compared to a standard of known fluorescence QY. The standard used in our study was rhodamine in ethanol, and its $QY_{F\ (Std)}$ was around 0.95.

The QY_F was estimated using equation 3:

$$QY_F = QY_{F(Std)} \frac{F\ A_{Std}\ n^2}{A\ F_{Std}\ n^2_{Std}} \tag{3}$$

Where F_{Std} and F are emission intensity of rhodamine and QDs at the excitation wavelength 380 nm respectively. A_{Std} and A are the absorbance of rhodamine and QDs respectively, while n is the refractive indices of water and n_{Std} is the refractive indices of ethanol.[22] The emission and absorption spectra of rhodamine are shown in Figure 2. For the uncoated CdTe QDs, the fluorescence QY value was 28.30%, and the fluorescence QY increased to 98.9% after the formation of the ZnS shell at the reflux time of 30 min, followed by a decrease to 64.80% after 120 min reflux time. Thus, the best time for synthesis is 30 min (Figure 3).

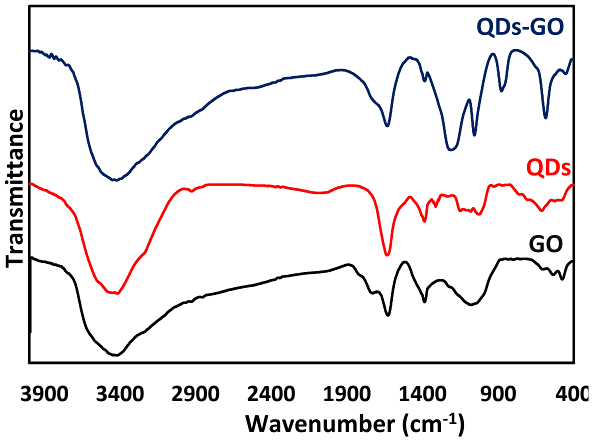

Figure 9. *FT-IR spectra of GO, unconjugated QDs, and QDs–GO nanocomposite.*

FT-IR measurements showed the successful bonding of TGA and MPA ligands on the QDs surface. In Figure 4, the absorption bands at 3450, 1583, 1389, 2900, 1325, and 3000-3300 cm^{-1} in the FT-IR spectrum of CdTe and CdTe/ZnS were clearly observed. The broad and strong peak at 3450 cm^{-1} is assigned to O–H stretching vibrations of the surface carboxylic acid functional groups on the QDs structure. The peaks at 1583 and 1389 revealed the symmetric and asymmetric carboxylic functional group ($\vartheta_{C=O}$ =1389 and 1583 cm^{-1}). The peak at 2900 cm^{-1} is assigned to C-H stretching vibrations.[23] The absence of the –SH peak in the 2500–2600 cm^{-1} region, of the QDs indicated the making of a new S–Cd bond with the Cd–thiolate complex on the surface of TGA-CdTe. Similarly, the absence of a –SH peak in the QDs in the 2500–2600 cm^{-1} region, indicated the cleavage of the thiol moiety. In addition, the stretching vibration of the N–H could appear at 3000–3300 cm^{-1}.[24]

The HRTEM image in Figure 5 revealed the structure and diameter of the aqueous GSH-CdTe/ZnS QDs. It was pretty evident that the nanoparticles' shape has approximately been spherical. According to previous studies, a compressive ZnS layer wrapped the CdTe core, which formed a lattice-mismatched Type-I core/shell heterostructure QDs could acquire high-quality luminescent properties.

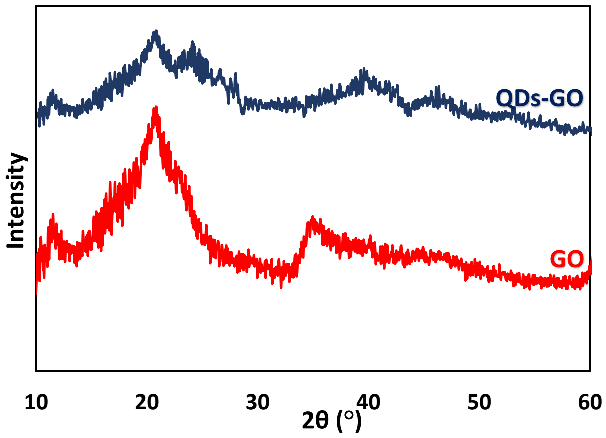

Figure 10*. XRD spectra of GO and QD-GO.*

Figure 6 shows the representative fluorescence emission of the un-conjugated GHS-CdTe/ZnS QDs (measured before conjugation to GO) and the QDs– GO nanocomposite. It can be seen that the emission spectra of the QDs–GO blue-shifted by 9 nm relative to the unconjugated QDs and also enhanced. The blue-shift in emission spectra of the QDs–GO indicated that the QDs were not aggregated and that the covalent binding of GO to the QDs increased the bandgap. Förster resonance energy transfer (FRET) from the QDs (donor) to GO (acceptor) is the sole reported mechanism of interaction between GO and fluorescent emitting QDs.

The morphology of the pristine components was analyzed with scanning electron microscopy. Figure 7 represents a typical field emission scanning electron microscopy (FESEM) image of GO nanocomposites. The photo shows a more disordered structure of GO than the ordered graphite flakes, which is due to the presence of various oxygen functional groups on the surfaces and edges of GO. The images show a more open structure of GO, and the outer layers are ready to exfoliate into the matrices to give better dispersion.[20]

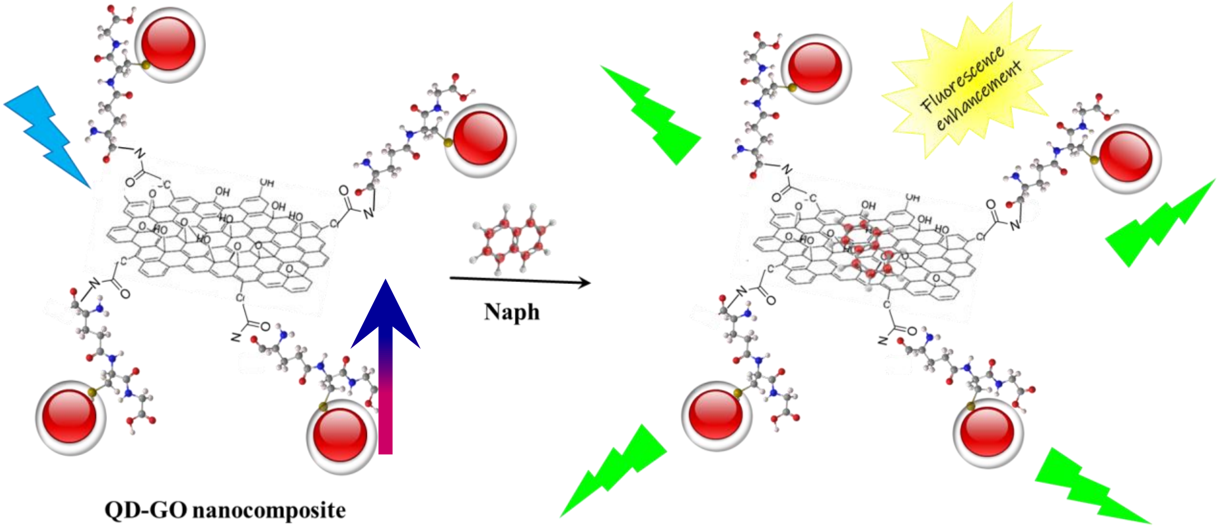

Scheme 2. *Fluorescence enhancement mechanism of naphthalene using the QDs–GO nanocomposite probe.*

Figure 8 shows the UV/Vis spectra of GO, the peak at 215 nm is π → π* transition due to C=C bonding is an aromatic ring, whereas the broad shoulder peak at 291 nm is n → π* transition due to C-O bonding. The absorption over 291 nm is expected to be caused by the conjugated fused ring plane, this indicates an sp^2-π conjugated network.[25, 26]

FT-IR analysis was carried out to characterize the functional groups on the surface of the materials. Figure 9 shows the FT-IR spectra of the GO, unconjugated QDs, and QDs–GO. GO has a peak at 1081 cm^{-1} attributed to the C-O bond, confirming the presence of oxide functional groups after the oxidation process. The peaks in the range of 1630 cm^{-1} to 1650 cm^{-1} show that the C=C bond remained before and after the oxidation process. The absorbed water in GO is shown by a broad peak at 2885 cm^{-1} to 3715 cm^{-1} contributed by the O-H stretch of H_2O molecules. The peak in 1722 cm^{-1} shows stretching vibration of C=O groups at the edges of GO.[18,20] The FT-IR spectrum of the unconjugated QDs revealed the symmetric and asymmetric carboxylic functional group ($\vartheta_{C=O}$ =1389 and 1583 cm^{-1}). These were ascribed to the capping agent. In terms of the QDs–GO nanocomposite, the FT-IR spectrum was dominated by the GO. However, the band appearing at around 1700 cm^{-1} could be attributed to the formation of the amide linkage between the QDs and GO.

XRD analyses were carried out to investigate the crystal phase nature of the unconjugated QDs, GO, and QDs–GO nanocomposite, respectively, see Figure 10. The diffraction pattern of GO revealed the presence of [001]; 2θ = 11.6° which was an indication of its characteristic loose-layer-like structure. The interlayers pacing of this peak depends on the water layers in the gallery space of the materials and the adopted method of preparation.[17] For the unconjugated QDs (not shown), the diffraction pattern suggested crystalline nature and corresponded to the typical zinc-blende crystal structure with planes, [111]; 2θ = 24°, [220]; 2θ = 40°, and [311]; 2θ = 45°. Upon conjugation of the QDs to GO, it was evident that the crystallinity of the QDs in the nanocomposite material was retained with no appreciable shift in the peak positions, and a weak GO peak in the QDs–GO spectrum was observed. This gave a strong indication that the QDs were well immobilized in the GO sheet.

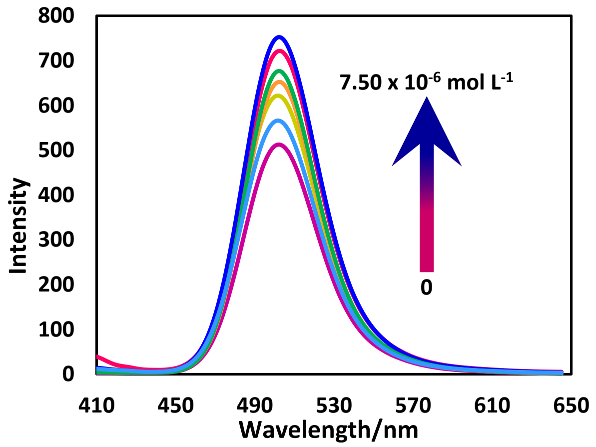

Figure 11. *Fluorescence detection of naphthalene at increasing concentration corresponding to a steady enhancement in emission signal of the QDs–GO probe, λ_{ex} =380 nm.*

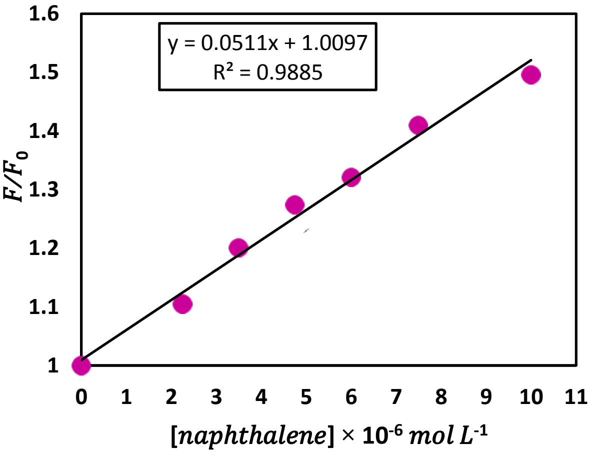

Figure 12. *Calibration curve showing the linear response of the QDs–GO probe upon detection of naphthalene. The concentration of GSH-CdTe/ZnS QDs was 8.8 × 10^{-6} M, GO was 5.00 mg L^{-1}, in PBS 0.025 mol L^{-1} (pH 7.5), room temperature and λ_{ex} =380 nm.*

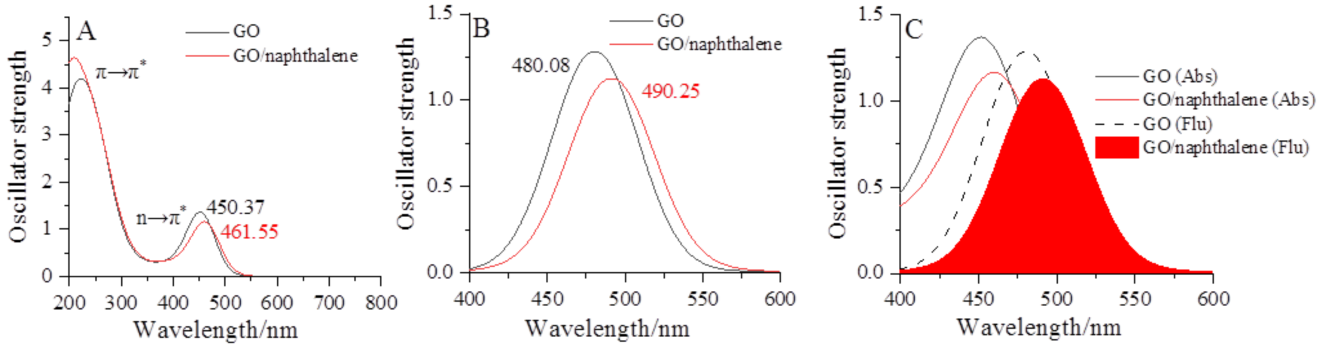

Figure 13. *Calculated UV/Vis absorption* ***(A)*** *and fluorescence emission* ***(B)*** *spectra for GO and GO/naphthalene systems at TD-DFTB level and the use of Quasinano 2015 parameters.* ***(C)*** *The overlap between the emission and absorption areas.*

Fluorescence detection of naphthalene

As discussed in the experimental section, GO was obtained via the chemical exfoliation of graphite oxide. It is important to note that breakage of the extended two-dimensional stacked π-conjugation of the graphene due to the oxidation results in hybridized sp^2 nanoscale graphitic domains which are surrounded by defect carbon vacancies as well as oxidized and highly disordered sp^3 domains. The resultant GO nanosheets were characterized by hydroxyl and derivatized carboxylic groups at the edges.[27-29] Based on this chemical functionality of GO, then nanosheets were readily exfoliated to form a light brown colored, stable, and dispersible suspension in water, which was required for the use of the QDs–GO as a material for the sensing of naphthalene in water. The advantage of using GO was not only limited to its large surface area but also was based on the nature of the chemical structure of GO. The strong π–π interaction induced by the hexagonal array of carbon atoms in the GO nanosheets provides a unique platform to adsorb analytes with fused benzene rings. We employed an equilibration time of 5 min before taking each of the fluorescence measurements. Naphthalene has fused benzene rings, hence enhancing their affinity for the QDs–GO probe (Scheme 2). Under optimum conditions in terms of the absence of matrix or interfering analytes, the detection of naphthalene using the QDs–GO probe was carried out at varying concentrations of the analyte. As shown in Figure 11, the emission intensity of the QDs–GO probe at 502 nm was progressively enhanced as the various concentration of naphthalene was increased.

The linear regression curve for detecting naphthalene is shown in Figure 12, with the concentration of the analyte in the range of 0.00 – 7.5 x 10^{-6} mol L^{-1}. The limit of detection (LOD) was calculated using the equation 3δ/K, where K is the slope of the calibration graph, and δ is the standard deviation of blank measurements (n=10). The LOD obtained for naphthalene was thus 7.71 x 10^{-8} mol L^{-1} which indicated that this method is useful for naphthalene detection.

Theoretical studies of sensing mechanism of the fluorescent probe

To understand the interaction mechanism between naphthalene and GO that leads to turn-on fluorescence, we have analyzed the energy decomposition analysis (EDA) for the naphthalene/GO complex. The complex has an interaction energy of -105.77 kcal/mol, consisting of electrostatic interaction of -79.71 kcal/mol, a Pauli repulsion of 48.92 kcal/mol, and an orbital interaction of -18.80 kcal/mol. The orbital interaction is decomposed into contributions from n and π orbitals of GO and π orbitals of naphthalene. Using time-dependent DFTB, we calculate UV/Vis absorption and fluorescence emission spectra of GO in the absence and presence of naphthalene. According to Figure 8, the absorption spectrum of GO shows two important peaks at 450.37 nm (assigned to n→π*) and 251.15 nm (assigned to π→π*) by contributions of 52.0 and 15.4% of total absorption. In the presence of naphthalene, the n→π* peak shows ca. 11 nm red shift to 461.55 nm. In addition, the calculated fluorescence emission spectrum of GO shows a peak at 480.08 nm, which can significantly overlap with the n→π* absorption area. This overlap can significantly reduce GO fluorescence emission, but the emission will not quench completely. The overlap of the small residual emission of GO at 480.08 nm with the QDs emission at ca. 500 nm could be the reason for the observed emission enhancement and the small blue shift for QDs–GO in Figure 6 (*see experimental section*).

In the presence of naphthalene, GO emission shows ca. 10 nm red shift to 490.25 nm. This peak is far away from the n→π∗ absorption area (**Error! Reference source not found.** 13C), something that reduces the overlap probability between GO emission and n→π∗ absorption area and prevents GO/naphthalene emission from quenching. Therefore, the overlap between the significant GO/naphthalene emission at 490.25 nm with the QDs emission at ca. 500 nm leads to the observed fluorescence enhancement in Figure 11 (*see experimental section*).

Conclusion

In summary, GSH-capped CdTe/ZnS core/shell QDs were synthesized and covalently bonded to GO, making a novel QDs–GO nanocomposite probe. The QD–GO nanocomposite probe was characterized using different techniques. Compared to unconjugated QDs, the fluorescence spectra of the QDs–GO nanocomposite illustrated the enhancement relative to the former. Results showed that the fluorescence enhancement effect was suitable for naphthalene, thus it was selected for further fluorescence studies. Detection of naphthalene was successfully carried out in aqueous media with a LOD of 7.71 x 10^{-8} mol L^{-1}. The simplicity, low cost, and low LOD of the sensor exhibit its potential for application as a screening tool for PAHs compounds in environmental water pollution monitoring.

Aknowledgement

Hereby, we extend our gratitude to the Research Council in Razi University of Kermanshah, Iran for its support financially in this research.

References

1. L.Wang, Y. Shen, Sh. Liu, J. Yang, W. Liang, D. Li, and Y. He, *Spectrochim. Acta, Part A*, 136, **2015**, 1607.
2. H.I Abdel-Shafy and M.S.M. Mansour, *Egypt. J. Pet.* 25, **2016**, 107.
3. M.J. Jacob, W. Karcher, R. Dumler, J.J. Belliardo, and A. Boenke, *J. Anal. Chem.,* 340, **1991**, 755.
4. Y. Kameda, J. Shirai, T. Komai, J. Nakanishi, and S. Masunaga, *Sci. Total Environ.,* 340, **2005**, 71.
5. S. Kumar, S. Negi, and P. Maiti, *Environ. Sci. Pollut Res*., 24, **2017**, 25810.
6. X. Wang, B. Liu, Q. Lu, and Q. Qu, *J. Chromatogr. A,* 1362, **2014**, 1.
7. S. Chowdhury and R. Balasubramanian, *Adv. Colloid Interface Sci*., 204, **2014**, 35.
8. S. Basu and P. Bhattacharyya, *Sens. Actuators B: Chem*., 173, **2012**, 1.
9. M. Alibolandi, F. Hadizadeh, F. Vajhedin, K. Abnous, and M. Ramezani, *Mater. Sci. Eng. C- Mater. Biol. Appl.,* 48, **2015**, 611.
10. M. Li, X. Zhou, S. Guo, and N. Wu, *Biosens. Bioelectron*., 43, **2013**, 69.
11. G. Zhiguo, Y. Shuping, L. Zaijun, S. Xiulan, W. Guangli, F. Yinjun, and L. Junkang, *Electrochim. Acta,* 56, **2011**, 9162.
12. F. Neese, The ORCA program system. *Wiley Interdiscip. Rev.: Comput. Mol. Sci.*, 2, **2012**, 73.
13. E. Glendening, et al., NBO, version 3.1; Gaussian. Inc.: Pittsburgh, PA, **2003**.
14. B. Hourahine, B. Aradi, V. Blum, F. Bonafé, A. Buccheri, C. Camacho, C. Cevallos, M.Y. Deshaye, T. Dumitrică, A. Dominguez and S. Ehlert, *J. Chem. Phys.*, 152, **2020**, 124101.
15. A.F. Oliveira, P. Philipsen, and T. Heine, *J. Chem. Theory Comput.*, 11, **2015**, 5209.
16. M. Wahiduzzaman, A.F. Oliveira, P. Philipsen, L. Zhechkov, E. Van Lenthe, H.A. Witek, and T. Heine, *J. Chem. Theory Comput.*, 9, **2013**, 4006.
17. P. Bhawal, S. Ganguly, T.K. Chaki, and N. C. Das, *RSC Adv*., 6, **2016**, 20781.
18. B. Lavakusa, B.S. Mohan, and P.D. Prasad, *Int. J. Adv. Res*., 5, **2017**, 405.
19. K.E. Sapsford, I.L. Medintz, J.P. Golden, J.R. Deschamps, H.T. Uyeda, and H. Mattoussi, *Langmuir*, 20, **2004**, 7720.
20. O. Adegoke and P.B.C. Forbes, *Talanta*, 146, **2015**, 780.
21. S. Maiti, T. Debnath, P. Maity, and H.N. Ghosh*, J. Phys. Chem. C*, 119, **2015**, 8410.
22. O. Adegoke and T. Nyokong, *J. Lumin*., 134, **2013**, 448.
23. A.V. Marenich, C.J. Cramer, and D.G. Truhlar, *J. Phys. Chem. B,* 113, **2009**, 6378.
24. D. Saikia, S. Chakravarty, N.S. Sarma, S. Bhattacharjee, P. Datta, and N.C. Adhikary, *Luminescence,* 32, **2016**, 401.
25. B. Lavakusa, B.S. Mohan, and P.D. Prasad, *Int. J. Adv. Res*., 5, **2017**, 405.
26. F.Y. Ban, S.R. Majid, N.M. Huang, and H.N. Lim, *Int. J. Electrochem. Sci*., 7, **2012**, 4345.
27. A. Lerf, H. He, M. Forster, and J. Klinowski, *J. Phys.Chem. B*, 102, **1998**, 4477.
28. W. Gao, L.B. Alemany, L. Ci, and P.M. Ajayan, *Nat. Chem*., 1, **2009**, 403.
29. W.S. Hummers Jr. and R.E. Offeman, *J. Am. Chem. Soc*., 80, **1958**, 1339.